JOURNAL OF MATERIALS SCIENCE **39** (2004) 1419– 1423

# Interlaminar fracture toughness and the associated fracture behavior for glass fiber reinforced polymers (GFRP)

T. KUBOKI*,‡, P.-Y. B. JAR*, J. J. R. CHENG‡
*Department of *Mechanical Engineering and ‡Civil & Environmental Engineering, University of Alberta, Edmonton, Alberta, T6G 2G8, Canada*
*E-mail: tkuboki@ualberta.ca*

Laminated fiber reinforced polymers (FRP) have excellent in-plane stiffness and strength, but suffer from transverse impact loading due to the lack of fiber reinforcement in that direction. Under transverse impact, extensive delamination can occur in the interlaminar resin-rich regions, which leads to a reduction of stiffness and strength. Therefore, many researchers have attempted to establish a standard testing method that characterizes the interlaminar fracture toughness for delamination [1]. In addition to the measurement of the delamination toughness, analysis of the fracture surface using optical microscopy or scanning electron microscopy (SEM) can also provide useful information for the delamination resistance characterization.

Recently, we have evaluated mechanical properties of two glass-fiber-reinforced polymers (GFRP) [2], using transverse impact, double cantilever beam (DCB) and end-notched flexure (ENF) tests. Results from the transverse impact and DCB tests showed a clear difference in delamination resistance between the two GFRP, but such a difference was not found from the ENF test. Based on the ENF test results, the two GFRP should have similar delamination resistance in the shear mode (Mode II). Although this discrepancy in delamination resistance may be caused by the toughness variation in different modes of loading, we believe that the discrepancy is mainly due to a problem with the ENF test for the characterization of the delamination resistance. This issue has been raised in several studies [3, 4], and is further investigated here through the examination of fracture surfaces to provide additional evidence.

Two GFRP used in this study have polymer matrices that are the same as those used previously, that is, isophthalic polyester (TMR300 isopolyester, provided by Viking Plastics, Edmonton) and polyurethane-based resin (PUL-G polyurethane, provided by Resin System Inc., Edmonton). The PUL-G polyurethane resin contains 15% $CaCO_3$ particulates for stiffness enhancement. For convenience, the two GFRP will be named PI-GFRP and PU-GFRP in this paper, for isopolyester-based GFRP and polyurethane-based GFRP, respectively.

The glass fiber used is 9-oz/yd$^2$ warp, unidirectional woven fabric (provided by ZCL Composites, Edmonton) which consists of parallel fiber bundles stitched together with a gap of around 1 mm. The gap between the fiber bundles generated resin-rich zones in the GFRP. Therefore, the GFRP have resin-rich zones in the intra-laminar, inter-fiber-bundle regions and the interlaminar regions.

GFRP plates of nominally 6.0 mm thick were fabricated using a resin transfer molding (RTM) technique. The fiber lay-up of the transverse impact specimens is $[(0/90)_5]_s$, and that of the DCB and ENF specimens is $[(0/90)_4 0_2]_s$ of which the four central 0-degree layers were to provide a uni-directional fiber environment in the direction of crack growth, in accordance with most of the test coupons used in the past. The specimens for DCB and ENF tests contain an aluminum insert film, 15 $\mu$m thick, that is placed between the 2nd and the 3rd of the four central layers, acting as a starting defect for delamination crack growth. Dimensions of the specimens are 93 $\times$ 93 mm$^2$ for the transverse impact test, and 120 $\times$ 20 mm$^2$ for the DCB and ENF tests. Overall fiber volume fraction of the specimens is around 40%, estimated using the following equation [5]:

$$\%V_{\mathrm{f}} = \frac{\mathrm{FAW} * N * 100}{\mathrm{FD} * 2\,h}$$

where FAW is the area weight of the fiber fabric (9 oz/yd$^2$ or 0.3046 kg/m$^2$), $N$ is the number of fiber layers (equal to 20 in this study), FD is the fiber density (2560 kg/m$^3$), and 2 h is the specimen thickness (0.006 m). Due to the shrinkage of isophthalic resin after curing, the fiber volume fraction of PI-GFRP is slightly higher than that of PU-GFRP, but the difference is insignificant.

The transverse impact tests were conducted at a speed of 5 m/s using an Instron Dynatup H8250 instrumented impact tester. The cylindrical steel striker has a hemispherical nose of 12.7 mm in diameter. Total mass of the striker assembly is 2.69 kg. The specimen was firmly clamped using a pneumatic clamping device, provided by Instron, which has a central circular hole, 76.2 mm in diameter. Test procedures for the DCB and ENF tests followed the protocols from the European Structural Integrity Society [5], and were conducted using an Instron Universal Testing Machine. The crosshead speeds for the DCB and ENF tests were 1.28 and 2.56 mm/min, respectively. Data deduction for critical strain energy release rates, $G_{\mathrm{Ic}}$ (Mode I) from the DCB test, and $G_{\mathrm{IIc}}$ (Mode II) from the ENF test, also followed the procedures recommended in the protocol. Table I summarizes the mechanical test results, that is, total absorbed energy from the transverse

  

TABLE I Summary of total absorbed energy under the impact, $G_{IC}$ values from DCB test and $G_{IIC}$ values from ENF test

| | Total absorbed energy under transverse impact (J) | $G_{IC}$ (J/m$^2$) | | | $G_{IIC}$ (J/m$^2$) | | |
|---|---|---|---|---|---|---|---|
| | | Non-linear[a] | 5% offset[b] | Propagation[c] | Non-linear[a] | 5% offset[b] | Maximum[d] |
| PI-GFRP | 20.5 | 440 | – | 610 | 2750 | 3590 | 3530 |
| PU-GFRP | 20.1 | 1600 | 2350 | 3270 | 2770 | 3520 | 3630 |

[a]Non-linear: The first non-linear point on the load-displacement curve.
[b]5% offset: The point from the 5% offset of the initial slope.
[c]Propagation: The point within the plateau region of the resistance curve (R-curve).
[d]Maximum: The point at the maximum force.

impact test, $G_{Ic}$ from the DCB test and $G_{IIc}$ from the ENF test. As expected, the two GFRP have a similar level of the total energy absorbed under transverse impact, very different $G_{Ic}$ values, and similar $G_{IIc}$ values.

Overall appearance of the damage generated by the transverse impact is presented in Fig. 1. Opacity of the damaged region is mainly due to the delamination cracks that were developed in interlaminar resin-rich regions. The photographs in Fig. 1 clearly show that the damage in PU-GFRP is less extensive than that in PI-GFRP. Since the specimens were tested under the same impact conditions and absorbed the same level of energy for damage development, the results in Fig. 1 suggest that PU-GFRP is tougher than PI-GFRP under the transverse impact.

SEM samples for fracture surface examination were selected near the central region, as indicated by the arrow in Fig. 1, within 6 layers from the back surface, that is, 25% of the thickness, to ensure that the samples

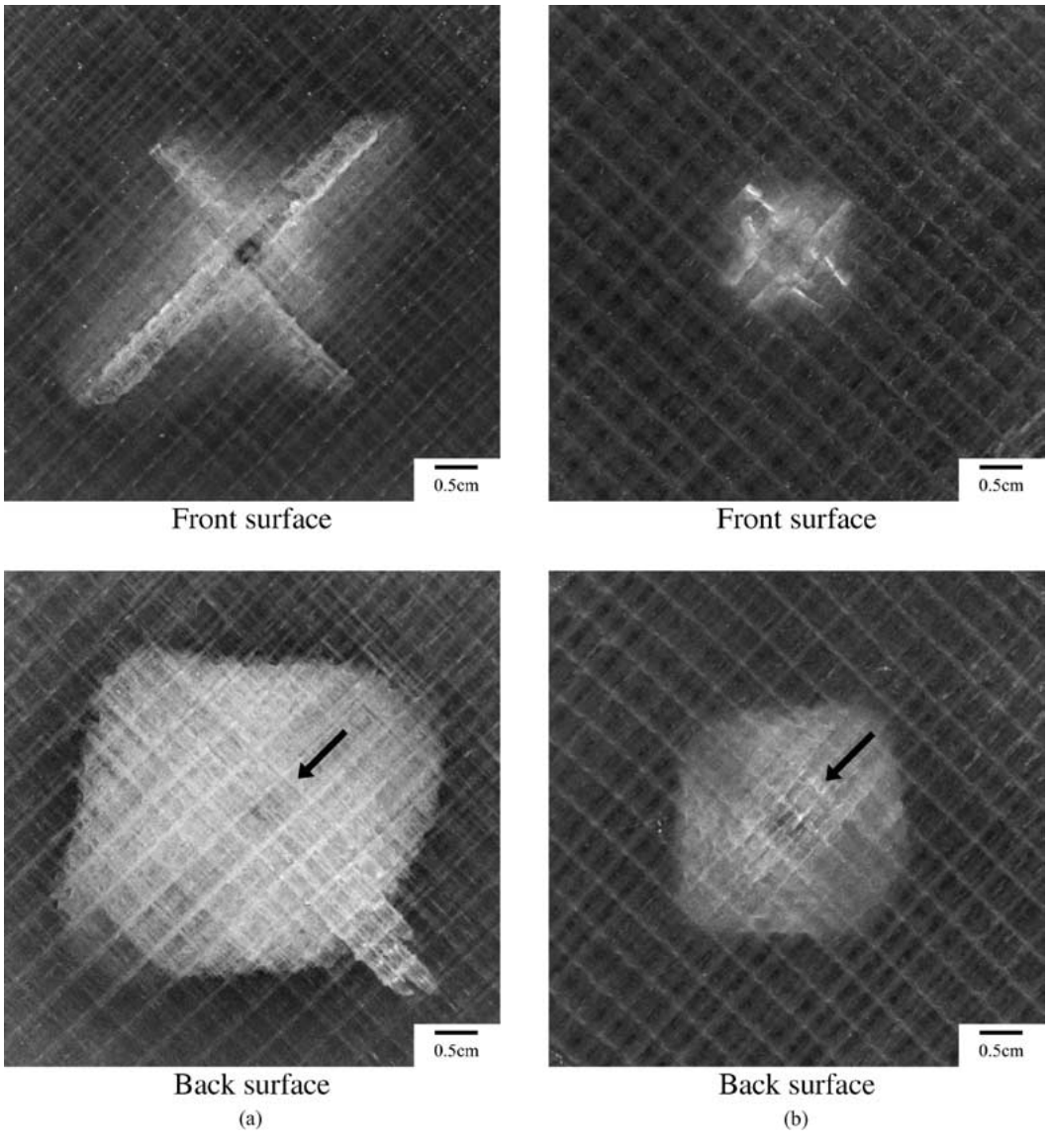


*Figure 1* Photographs of the transverse impact damaged specimens, at a speed of 5.0 m/s: (a) PI-GFRP and (b) PU-GFRP. The surface contacted with the striker is called the "front surface," and the other surface the "back surface." Arrows on the figure indicate the region of the first layer underneath the back surface" where SEM micrographs in Fig. 2 were taken.

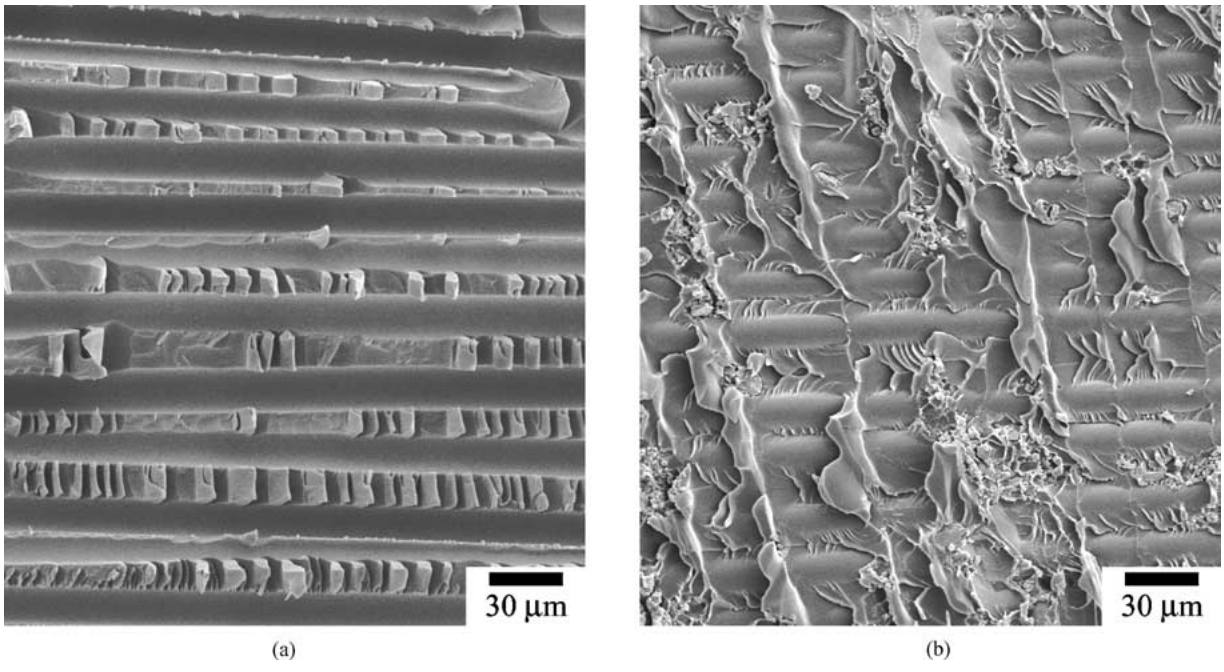


*Figure 2* SEM micrographs of the delamination surface of the transverse impacted specimens: (a) PI-GFRP and (b) PU-GFRP.

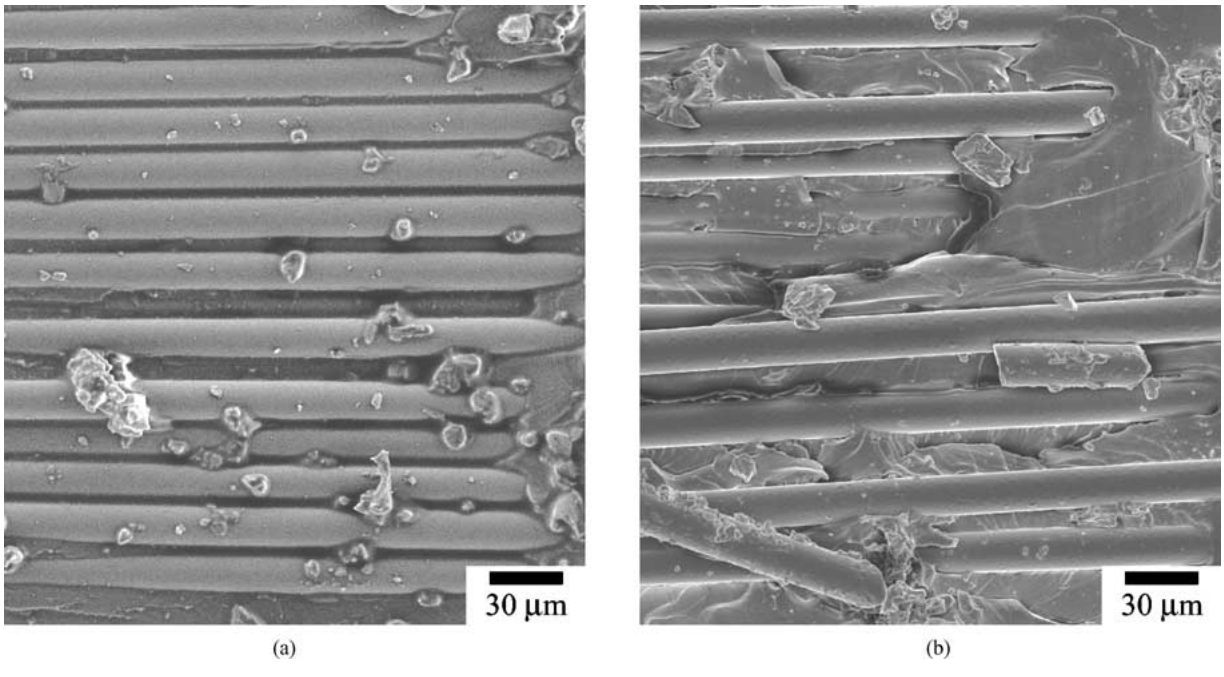


*Figure 3* SEM micrographs of the delamination surfaces of the DCB specimens: (a) PI-GFRP and (b) PU-GFRP.

were taken from the sections that contain extensive delamination. The SEM samples were firstly coated with a thin layer of gold, and then examined using a scanning electron microscope (Hitachi S-2500 SEM). Typical micrographs are presented in Fig. 2. Fig. 2a, from PI-GFRP, shows bare fibers with hackle marks in between. Based on our experience, this is a typical brittle fracture under Mode II loading, showing poor bonding at the fiber-matrix interface. On the other hand, Fig. 2b, from PU-GFRP, contains fine hackle marks and relatively extensive matrix deformation. Fig. 2b also contains imprints of cross fibers above the interlayer where the delamination occurred. All of these behaviors indicate that PU-GFRP has a stronger resistance to the crack growth than PI-GFRP, which is consistent with conclusions from the mechanical test results.

According to the studies conducted by Masters [6] and Hiley [7], the observation of hackle marks on the fracture surface is an indication of shear deformation during the delamination process. Therefore, the interlaminar fracture of the GFRP under transverse impact is most likely to be under deformation in Mode II.

Typical fracture surfaces of the DCB specimens are shown in Fig. 3. Fig. 3a, from PI-GFRP, shows a very flat feature that is covered mainly by bare fibers with little deformation in the surrounding matrix. On the other hand, Fig. 3b, from PU-GFRP, shows more significant matrix deformation with some fibers covered by residual matrix. Fiber fracture was also

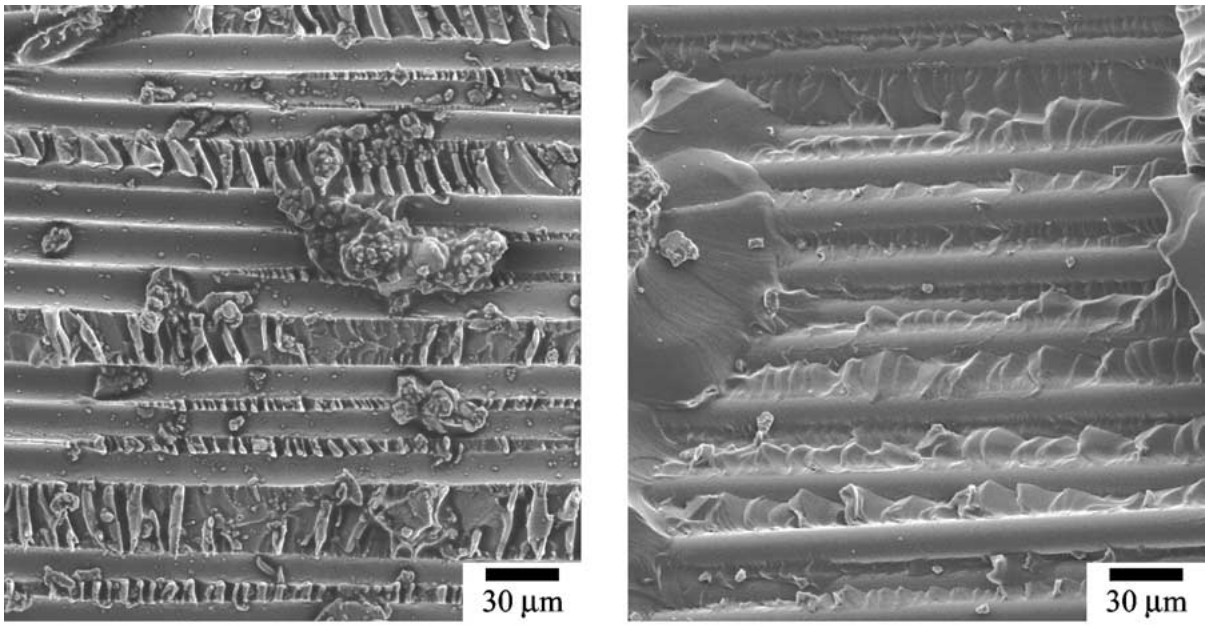


*Figure 4* SEM micrographs of the delamination surface of the ENF specimens: (a) PI-GFRP and (b) PU-GFRP.

found on the surface of Fig. 3b, indicating the occurrence of fiber bridging during the fracture process [1]. The micrographs in Fig. 3 suggest that for the two GFRP under Mode I loading, PU-GFRP shows better interfacial bonding between the fiber and the matrix and has a stronger resistance to crack growth.

Typical fracture surfaces of the ENF specimens are presented in Fig. 4. Fig. 4a, from PI-GFRP, contains regular hackle marks with bare fiber surface, but Fig. 4b, from PU-GFRP, shows a relatively extensive matrix deformation with improved bonding between the fiber and the matrix. Since these micrographs show a similar difference in the fracture process to those shown in Fig. 2, we believe that these micrographs also suggest that PU-GFRP has a better resistance to Mode II delamination crack growth than PI-GFRP.

The above SEM observations suggest that PU-GFRP is tougher than PI-GFRP in all three modes of loading, that is, under transverse impact, Mode I delamination and Mode II delamination. The conclusion is consistent with the mechanical test results from transverse impact and DCB tests, but inconsistent with the results from the ENF test, which did not show any significant difference between PI-GFRP and PU-GFRP.

Further investigation into the ENF test results suggests that the difference between PI-GFRP and PU-GFRP on the load-displacement curves occurs only after the point of the maximum load, as shown in Fig. 5 in which PI-GFRP shows a sudden drop of the load due to unstable crack growth but PU-GFRP shows first a gradual decrease of the load due to relatively stable crack growth before the occurrence of the unstable crack growth. It is believed that the difference in fracture surfaces shown in Fig. 4 reflects the difference of the load-displacement curves after the point of the maximum load. Since all $G_{\mathrm{IIc}}$ values in Table I were calculated based on points before or at the

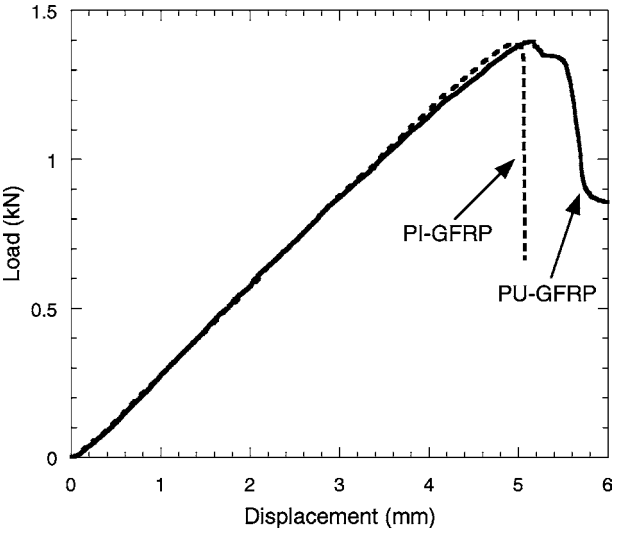


*Figure 5* Typical load-displacement curves for the ENF tests.

point of the maximum load ($G_{\mathrm{IIc,non\text{-}linear}}$ and $G_{\mathrm{IIc,5\%}}$ for the former and $G_{\mathrm{IIc,max}}$ for the latter), these values cannot show the difference in the fracture process that mainly occurred after the point of the maximum load.

In conclusions, this study presents SEM observation to support that PU-GFRP has higher toughness than PI-GFRP, due to good interfacial bonding between the fiber and the matrix and significant plastic deformation of the matrix during the crack growth process. This conclusion is consistent with the mechanical test results from DCB and transverse impact tests.

The study also found that the $G_{\mathrm{IIc}}$ values derived from the ENF test failed to show the difference in the crack growth resistance between PI-GFRP and PU-GFRP. Therefore, results from the ENF test should be treated with caution when used for evaluation of delamination resistance for fiber composites.

## Acknowledgments

The work was sponsored by ISIS Canada and the Natural Science and Engineering Research Council of Canada (NSERC)—Research Grant Scheme. We are grateful to Dr. Ming H. Chen, in Medicine/Dentistry Electron Microscope Unit, University of Alberta for the technical assistance.

## References

1. T. K. O'BRIEN, *Composite* Part B **29B** (1998) 57.
2. T. KUBOKI, P.-Y. B. JAR and T. W. FOREST, *Comp. Sci. Tech.* **63** (2003) 943.
3. T. K. O'BRIEN, in "Composite Interlaminar Shear Fracture Toughness, $G_{IIC}$: Shear Measurement or Sheer Myth?," ASTM STP 1330, edited by R. B. Bucinell (American Society for Testing and Materials, 1998) p. 3.
4. M. TODO, P.-Y. B. JAR and K. TAKAHASHI, *Comp. Sci. Tech.* **60** (2000) 263.
5. Protocols for Interlaminar Fracture Testing of Composites. European Structural Integrity Society (ESIS), Delft, The Netherlands, 1993.
6. J. E. MASTERS, "Characterization of Impact Damage Development in Graphite/Epoxy Laminates," ASTM STP 948, edited by J. E. Masters and J. J. Au (American Society for Testing and Materials, Philadelphia, 1987) p. 238.
7. M. J. HILEY, *Plast. Rubb. Compo.* **28** (1999) 210.

*Received 19 June*
*and accepted 16 September 2003*